Fluorescence depolarization in poly[2-methoxy-5-((2-ethylhexyl)oxy)-1,4-phenylenevinylene]: Sites versus eigenstates hopping

Jaykrishna Singh,[1] Eric R. Bittner,[1,a)] David Beljonne,[2] and Gregory D. Scholes[3]
[1]*Department of Chemistry and Center for Materials Chemistry, University of Houston, Houston, Texas 77204-5003, USA*
[2]*Laboratory for Chemistry of Novel Materials, University of Mons-Hainaut, Place du Parc 20, 7000 Mons, Belgium*
[3]*Department of Chemistry, Institute for Optical Science, and Center for Quantum Information and Quantum Control, University of Toronto, Toronto, Ontario M5S 3H6, Canada*

(Received 13 July 2009; accepted 19 October 2009; published online 17 November 2009)

We report upon a theoretical study of singlet exciton migration and relaxation within a model conjugated polymer chain. Starting from poly[2-methoxy-5-((2-ethylhexyl)oxy)-1,4-phenylenevinylene] polymer chains, we assume that the π-conjugation is disrupted by conformational disorder of the chain itself, giving rise to a localized Frenkel exciton basis. Electronic coupling between segments as determined by the coupling between the transition densities of the localized excitons gives rise to delocalized exciton states. Using a kinetic Monte Carlo approach to compute the exciton transfer kinetics within the manifold of either the dressed chromophore site basis or dressed eigenstate basis, we find that the decay of the polarization anisotropy of the exciton is profoundly affected by the delocalization of the exciton over multiple basis segments. Two time scales emerge from the exciton migration simulations: a short, roughly 10 ps, time scale corresponding to rapid hopping about the initial excitation site followed by a slower, 180 ps, component corresponding to long range hopping. We also find that excitations can become trapped at long times when the hopping rate to lower-energy states is longer than the radiative lifetime of the exciton. © *2009 American Institute of Physics*. [doi:10.1063/1.3259549]

I. INTRODUCTION

The performance of conjugated polymers in optoelectronic devices such as light-emitting diodes, photodetectors, and solar cells is largely believed to be linked to the dynamic behavior of the primary photoexcitations.[1–6] The primary photoexcitations are difficult to address in the conjugated polymer because they are sensitive to the local structure and packing morphology of the polymer chains.[6–10] In the idealized sense, the conjugated network of a polymer may be formally extended over the entire polymer chain. However, in reality torsions and energetic disorder along the chain as well as chemical defects limit the persistence length of a given π-conjugated domain.[11,12] We can envision chopping a large conjugated polymer chain into a series of linked "chromophoric" units in which the electronic coupling between domains can be both through-space via Coulombic coupling and through-bond via coupling between C 2p orbitals of nearest neighbor segments.[13–15] This implies that the diffusion and mobility of an excitonic state through a conjugated polymer material will be determined by strong and weak electronic couplings. Therefore, a Förster hopping model may not adequately describe energy transfer in these materials.[9,16–18] One of the best probes of the ultrafast process of excitation energy transfer is to monitor the fluorescence depolarization as an exciton is transferred from one state (or chromophore site) to another.[19–21] Furthermore, energy transfer events are often assumed to be incoherent; however, recent evidence suggests quite strongly that quantum coherence effects may play an important role in energy transfer.[22,23]

In this paper, we address excitation energy transfer in a model conjugated polymer chain that has been decomposed into a series of linked chromophore segments. We consider two limiting regimes starting from a common Hamiltonian model. In the first case, we assume the electronic coupling between chromophore sites can be cast in the weak-coupling limit and transitions occur from one localized chromophore site to another. Here we can cast our model in the form of a spin-boson Hamiltonian treating the bare off-diagonal electronic coupling as the perturbation. In the second case, we take a more realistic stance and assume that transitions occur between vibronic eigenstates. This second case is more difficult from a theoretical point of view since the electronic perturbation is dressed by the phonons. In both cases we shall use a Fermi's golden rule approach to compute the site-to-site or state-to-state transfer rates. What we shall see is that there is a clear distinction between these two descriptions as evidenced by their respective predicted anisotropy decays even after averaging the results from multiple configurations and varying initial excitations.

II. THEORETICAL BACKGROUND AND METHODOLOGY

The starting point for our discussion is a model Hamiltonian given by

a)Electronic mail: bittner@uh.edu.

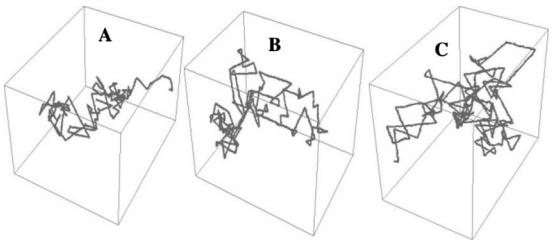

FIG. 1. Conformations of three representative PPV chains. The radii of gyration of chains are chain A: 300 Å, chain B: 210 Å, and chain C: 154 Å. Chain *A*, *B*, and *C* consists of 135, 145, and 150 respective number of effective PV chromophore units.

$$H = H_0 + V. \tag{1}$$

Here, H_0 includes all the terms that are diagonal in a basis of local excitations,

$$H_o = \sum_n \epsilon_n a_n^\dagger a_n + \sum_{ni} \left(b_{ni}^\dagger b_{ni} + \frac{1}{2} \right) \hbar \omega_{ni} a_n^\dagger a_n + \sum_{ni} (b_{ni}^\dagger + b_{ni}) \sqrt{\frac{\hbar}{8\omega_{ni}}} g_{ni} a_n^\dagger a_n, \tag{2}$$

and V includes the off-diagonal elements,

$$V = \sum_{n \neq m} \lambda_{nm} (a_n^\dagger a_m + a_m^\dagger a_n). \tag{3}$$

Indices n and m label individual chromophore segments of a much longer polymer chain with vertical energies ϵ_n and ϵ_m, respectively. The operators $\{a_n^\dagger, a_n\}$ create or remove local excitations on the nth chromophore segment; $b_{ni}^\dagger$ and b_{ni} are the boson creation and annihilation operators for the vibrational mode i of the nth chromophore segment with frequency ω_{ni}. Finally, λ_{nm} is the purely electronic interaction term between chromophore segment n and m. The off-diagonal couplings λ_{nm} are independent of the phonons and can be computed using quantum chemical methods. The terms involving $(b_{ni}^\dagger + b_{ni})$ represent displacement of equilibrium positions of the vibrational modes upon electronic excitation. Within a given chromophore segment, we assume that the exciton is coupled linearly to localized phonons with operators $\{b_{ni}^\dagger, b_{ni}\}$. Such vibronic coupling results in a distortion of the excited state upon relaxation and the linear coupling parameters $\{g_{ni}\}$ can be deduced from the Huang–Rhys factors in the vibronic (Raman) emission spectra. This is a general "molecular crystal" model used extensively by our group[24,25] and others.[26–31]

For the case of poly(phenylenevinylene) (PPV) chains, Dykstra *et al.*[16] generated a large number of model polymer chains based upon a random growth algorithm,[13,32] decomposed each of the chains into a series of independent chromophores, and computed the excitonic couplings using rigorous quantum chemical methods. Ensemble properties were obtained by averaging over all the generated configurations. To provide a relevant description of the system dynamics, we carefully examined only three representative PPV polymer chains. Here we adopt the conformations and parameters used in Ref. 16. The conformations of these three representative PPV chains are shown in Fig. 1. Polymer chains *A*, *B*, and *C* consist of 135, 145, and 150 effective chromophore segments, respectively. An effective chromophore segment, in general, known as a conformational subunit or light absorbing units, is composed of sizes ranging from 2 to 25 phenylenevinylene (PV) repeat units. For example, Fig. 2 shows the different shapes of conformational subunits denoted with unique color in the polymer chain *A*, *B*, and *C*. As illustrated, larger segment can have a central or side conjugation breaks. We assume each conformational subunit has three independent phonon branches with frequencies: $\omega_{n1} = 700\ \text{cm}^{-1}$, $\omega_{n2} = 1200\ \text{cm}^{-1}$, and $\omega_{n3} = 1600\ \text{cm}^{-1}$, respectively. These frequencies roughly correspond to the dominant ring torsions, C–C bond stretches, and C=C bond stretches, respectively, in a PPV polymer.[33,34] The linear electron-phonon couplings, g_{ni}, associated to each vibrational mode of chromophore segment n, are deduced from the Huang–Rhys factors in the vibronic emission spectra with $g_{n1} = 0.2$ for all n (similarly for $g_{n2} = 0.9$, $g_{n3} = 0.2$). In our study, we should stress that the vibrational frequencies (assumed) with corresponding Huang–Rhys factors for each segment length are sufficient enough to reproduce the main features of the absorption and fluorescence spectrum. From the theoretical point of view, a complete set of vibrational frequencies for all segment lengths has a limited influence because, at room temperature, the gross features of the absorption and fluorescence spectra appear identical with respect to change in the number of PV repeat units, except some additional shift extending to the red.[9]

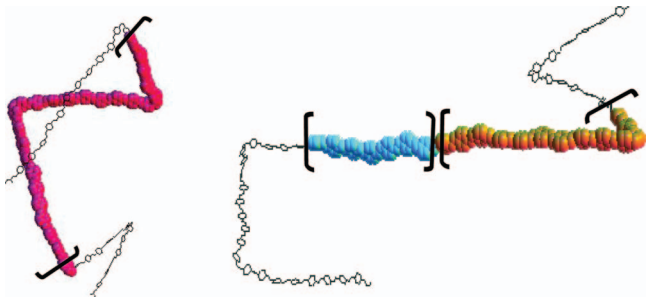

FIG. 2. Each bracket denotes conformational subunit (segment) with unique color, which represents the shape of segments in the part of the polymer chains *A*, *B*, and *C*. In our study, one large segment can have central conjugation breaks, it is mainly because these polymer chains can be "broken up" into segments with an acceptable cutoff (dihedral) angle. A cutoff of around 55° was typically used (Ref. 16). Reference 16 states that all of the segments are coupled and there is no discernible difference between one large segment with conjugation break or two smaller segments that are strongly coupled.

In the current model, the excitation is assumed to be delocalized over several conformational subunits. Before addressing energy transfer mechanisms, let us first examine the eigenstates given by our model system. In Fig. 3 we show the localization of the lowest six eigenstates of our system superimposed on polymer chain *A*. The color coding in each gives an indication of the individual chromophore subunits (i.e., basis sites) participating in each particular state colored according to the net amplitude contributed to that state. For example, as shown in Fig. 3, state #1 (inverse participation ratio, IPR=0.99) is delocalized through-bond over a contiguous "Z" shaped structure, which consists of 2–25 PV repeat

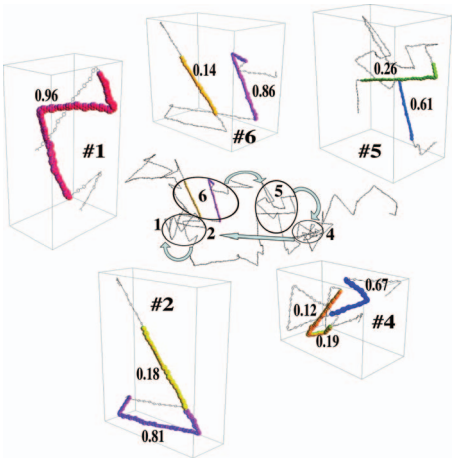

FIG. 3. Delocalization of electronic eigenstate in the dressed eigenstate representation as the primary excitation moves along the polymer chain A. Here, $(6\rightarrow5)$, $(5\rightarrow4)$, etc, represent exciton relaxation among eigenstates such as 6 to 5, 5 to 4. The coloration indicates the net amplitude of an exciton eigenstate. Only the significant portion of the amplitude of a state is colored. Less than 10% of the amplitude is not shown. The color coding is shown with its particular amplitude, which indicates the participation of individual chromophore subunits (i.e., basis sites). For state #4, the color coding indicates that 67%, 19%, and 12% of the amplitudes are delocalized over three different segments in which the first two of them has conjugation breaks. For state #6, the color coding indicates that 86% of the amplitude is delocalized over a segment that has a conjugation break and 14% of the amplitude delocalized on another segment. For state #1, the color coding indicates that 96% of amplitude is delocalized over one larger segment with conjugation breaks and 4% of the amplitude is delocalized over the rest of the segments in the chain which is not shown. Lower energy states are generally associated with larger segments, whereas shorter segments give rise to higher energy states.

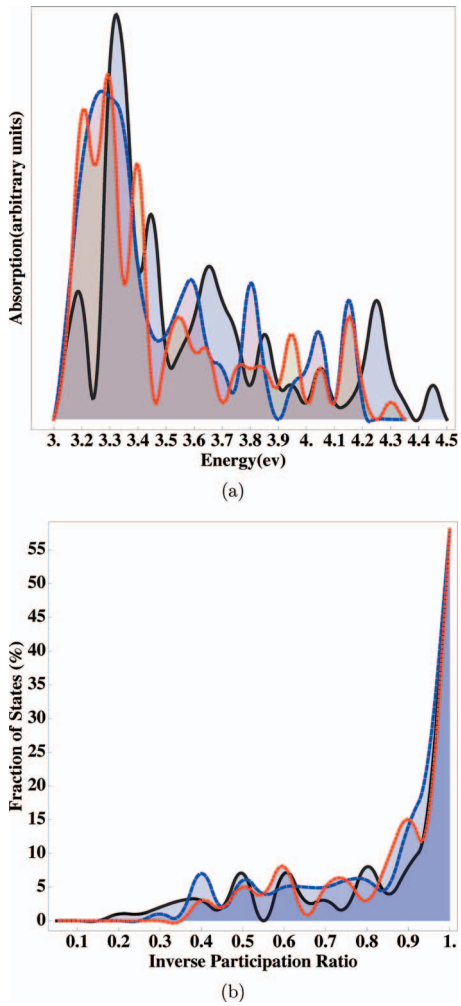

FIG. 4. Simulated absorption spectrum and inverse participation ratio for PPV polymer chains: chain *A*-dotted line (red), chain *B*-solid line (black), and chain *C*-dashed line (blue). There is no significant correlation between (a) absorption spectrum and (b) IPR. IPR represents continuous beta distribution function with a *p*-value equal to 0.05 (i.e., probability of observing a difference between sample and population is less than 0.5%). Mean and standard deviation of the beta distribution for each chain is chain A: (μ=0.84, σ=0.18), chain B: (μ=0.84, σ=0.21), and chain C: (μ=0.82, σ=0.20).

units. The color coding indicates that 96% of amplitude of the state #1 is delocalized over one larger segment that has conjugation breaks and 4% of the amplitude is delocalized over the rest of the segments in the chain, which is not shown. It does not imply that the probability is constant. Likewise state #2 (IPR=0.99) is delocalized through-bond over an "L" shaped structure in which the color coding indicates that 81% of the amplitude is delocalized over one segment and 18% of the amplitude is localized on another segment. On the other hand, states #4, #5, and #6 are delocalized both through bond and space over segments, where each conformational subunit consists of 2–25 PV repeat units. For state #4 (IPR=0.98), the color coding indicates that 67% of the amplitude is localized over one segment, and the rest of the amplitudes (19% and 12%) are localized over two different segments. For state #6 (IPR =0.99), the color coding indicates that 86% of the amplitude is delocalized over a segment that has a conjugation break and 14% of the amplitude delocalized on another segment.

In Fig. 4 we show the computed absorption spectra for each chain along with the IPRs for the vertical eigenstates of our model. The IPR is a measure of the extent of quantum delocalization over a set of basis states:[35,36]

$$\mathrm{IPR}(\alpha) = \sum_n |\phi_{\alpha n}|^4. \tag{4}$$

Here, $\{\phi_{\alpha n}\}$ are the projections of the exciton eigenstates $|\phi_\alpha\rangle$ on to the local chromophore basis $|n\rangle$,

$$|\psi_\alpha\rangle = \sum_n \phi_{\alpha n}|n\rangle. \tag{5}$$

For each chain, we obtain all eigenvalues ϵ_α and eigenstates $|\psi_\alpha\rangle$ by complete diagonalization of the Hamiltonian, Eq. (1). In general, the IPR ranges from 0.99 where the exciton is completely localized to at least one conformational subunit to 0.006 where the exciton is delocalized over the entire polymer chain.[35,36] In our study, the IPR data for all the states of the polymer chains are randomly distributed between 0.99 (localized over one segment) and 0.17 (delocalized over at least six segments), and it shows no significant correlation with absorption spectrum. As we can see from Fig. 4, the IPR plot for each chain represents beta distribution function with particular mean and standard deviation. For example, energy states of the polymer chain *C* are delocalized on average over 1.2 (IPR=0.82) segments with a standard deviation of five (IPR=0.20) segments. This indicates that by and large the exciton eigenstates are localized to

one or two chromophore "segments". Typically, the segments are over a contiguous section of the chain; however, in a large number of cases, the eigenstates are delocalized "through space" between neighboring segments that are not contiguously linked.

A. Kinetic Monte Carlo approach

In general, energy transfer dynamics within this system is most accurately described within the context of the quantum Liouville equation in which we propagate the reduced density matrix for the electronic states as coupled to a bath of oscillators held at fixed temperature, T. For small systems with only a few states, this is feasible; however, for a large, extended system such as the case at hand one needs to make a number of judicious approximations. First, we shall assume that energy transfer occurs *either* between the dressed electronic eigenstates or between the dressed individual chromophore sites. In both cases we shall assume that one can use a convolutionless Pauli master equation approach for propagating populations,[37]

$$\dot{P}_n(t) = \sum_m W_{nm}(t)P_m(t) - W_{mn}(t)P_n(t). \tag{6}$$

Here, $P_n(t)$ is the probability of finding the exciton on chromophore segment (or eigenstate) n at time t and $W_{nm}(t)$ are the time-dependent rates for transitions between chromophore segments (or eigenstates). Furthermore, we assume that we can take a golden-rule limit,

$$\lim_{t\to\infty} W_{nm}(t) = \bar{W}_{nm}, \tag{7}$$

in computing the state-to-state and chromophore segment-to-segment rates. The convolutionless master equation then reduces to the Pauli master equation,

$$\dot{P}_n(t) = \sum_m \bar{W}_{nm}P_m(t) - \bar{W}_{mn}P_n(t), \tag{8}$$

which we can solve upon specifying the rates and the initial conditions $\{P_n(0)\}$. Otherwise, one would have to apply master equation solutions with formally time dependent transition rates.[38,39] The central assumption here is that the time scale for energy transfer between the dressed eigenstates is larger than the decay time of the correlation function used in computing the rate constant $\bar{W}_{nm}$. In our model, the calculation of transfer rate $W_{\alpha\beta}$ [Eq. (29)] between state α and β takes ~21 h (on GNU/Linux ×86–64). It is mainly due to large number of summations involved at each time step $d\tau$ in the correlation function [Eq. (30)] that is propagated for long time. In order to propagate actual population $\dot{P}_n$ of an excitation in a given eigenstate n, we shall calculate $2(n\times n)$ transfer rates. For example, in a given PPV representative chain C that has 150 number of states, we shall compute 45 000 transfer rates, and it will take ~100 processor years. Given the number of states involved, we adopt a kinetic Monte Carlo (KMC) method[40,41] in which the exciton migration occurs in a stochastic manner and $P_n(t)$ is reproduced by averaging over multiple realizations. The KMC method works in the following way. Starting from a given initial chromophore segment site n, one picks a "target" site ($m \neq n$) among all other sites on the chain. We then calculate the golden-rule rate constant $\bar{W}_{nm}$, associated with the $n\to m$ transition and calculate mean waiting time for the excitation to remain on site n before hopping to the new site. This is justified by assuming a first order process with exponential decay statistics that gives the probability distribution of the mean time it takes to transfer the excitation from state n and m,

$$\bar{t}_{nm} = \frac{1}{\bar{W}_{nm}}. \tag{9}$$

In a sense, this is much the way we envision an individual experiment to proceed. In order to efficiently sample the hopping steps so that our random walk is biased toward making hops to new sites that are more strongly coupled to the old site, we apply Monte Carlo selection criteria based upon the electronic coupling between the segment (site) n and m. Again, we wish to avoid explicitly calculating all the $\bar{W}_{nm}$'s. Thus, instead of choosing our target state from a uniform distribution, we will bias our selection based upon states most strongly coupled to the current state using

$$p_{nm} \approx \frac{\lambda_{nm}^2}{\sum_m \lambda_{nm}^2}, \tag{10}$$

where p_{nm} is the probability of making a hop from the nth to the mth state, λ_{nm} is the bare electronic coupling between segment (site) n and m. In principle the p_{nm} are related to the rates $\bar{W}_{nm}$, subject to the normalization for an N site system. However, this does neglect the spectral overlap between donor and acceptor states and is biased in the sampling toward states with the longer subunits. To overcome this, the spectral overlap factors are properly accounted in determining the transition rates between states n and m. Consequently, if the state selection step is biased toward states with lower Franck–Condon factors, then the transition time to such a state would be longer. Therefore, the underlying biased sampling scheme generates more probable strongly coupled states. This is important because sampling at random with equal probability will result in energetically unfavorable hopping states.

The KMC algorithm[40] can be described as

(1) choose an initial state n in a localized or delocalized basis,
(2) calculate the discrete cumulative function $CF(n) = \Sigma_i p_{ni}$ for $i=1,\ldots,N$ where N is the total number of states,
(3) generate a uniform random number $r \in [0,1]$,
(4) evaluate $CF(m)=r$ and then hop to state m,
(5) calculate exciton transfer rate $\bar{W}_{nm}(t)$,
(6) evaluate $\{\bar{t}_{nm}\}=\bar{W}_{nm}^{-1}$, where $\{\bar{t}_{nm}\}$ is the mean time required to hop from state n to m. In other words, the average amount of time spent in state n before hopping to m; and

(7) we arrive at new state m, and then go to step (2). In a given simulation, one generates a list of hops between states $\{(n,m)\}$, exciton transfer rates $\{(\bar{W}_{nm}\}$, and mean time between hops $\{\bar{t}_{nm}\}$.

Figure 3 displays a representative sequence of the hopping of a single excitation within one of the chains (chain A) in the eigenstate representation. Here the exciton is arbitrarily initiated in state #6, which itself is delocalized over two parallel chromophore segments (highlighted on the chain). The exciton hops to state #5, which is located on a nearby segment of the polymer and continues to migrate through the polymer before eventually stopping in state #1. Over the course of a sequence of hops we compute the depolarization of the exciton's transition moment as it hops through the polymer chain. The depolarization for a given chain is realized by averaging 100 replication sets of calculations each starting from randomly selected state or site, where each replication includes 25–30 state-to-state or segment-to-segment hopping elements.

We next discuss the calculation of the golden-rule rates for transitions between the dressed chromophore sites and for transitions between the dressed eigenstates. For the case of transitions between dressed chromophore sites, we can use a standard molecular crystal approach for computing the site-to-site rates. However, for the case of hopping between the eigenstates, the electronic coupling also depends upon the phonon coordinates so that the standard prescription for computing rates no longer holds. In both cases, we start with the same Hamiltonian model [Eq. (1)] and use a polaron transformation to calculate the nuclear contributions.

B. Energy transfer rates within a dressed chromophore site representation

Within the molecular crystal model, we take the off-diagonal electronic coupling in Eq. (1) to be the perturbation while keeping the electron-phonon coupling terms on the diagonal. We review here briefly the derivation of the golden-rule rate for this case in order to compare to our derivation in the next section. We first perform the canonical polaron transformation in order to effect the change of equilibrium displacement,[27,42,43]

$$\tilde{H} = e^{is} \cdot H \cdot e^{-is}, \tag{11}$$

with the shift operator,

$$s = (-i)\sum_{n,i} \Phi_{ni}(b_{ni}^{\dagger} - b_{ni})a_n^{\dagger}a_n, \tag{12}$$

where

$$\Phi_{ni} = \frac{g_{ni}}{\hbar\omega_{ni}}\sqrt{\frac{\hbar}{8\omega_{ni}}}. \tag{13}$$

The effect of this transformation on the phonon coordinates is to shift the equilibrium positions from which vibrational displacements are measured.[28] The transformed Hamiltonian is given as[27]

$$\tilde{H} = \sum_{n,i} a_n^{\dagger}a_n\left[\left(b_{ni}^{\dagger}b_{ni} + \frac{1}{2}\right)\hbar\omega_{ni} + \tilde{\epsilon}_n\right] - \lambda_{nm}(a_n^{\dagger}\hat{G}_n^{\dagger}\hat{G}_m a_m + a_m^{\dagger}\hat{G}_m^{\dagger}\hat{G}_n a_n), \tag{14}$$

where the shifted chromophore site energies are given by

$$\tilde{\epsilon}_n = \epsilon_n - \sum_i \frac{g_{ni}^2}{8\omega_{ni}^2}, \tag{15}$$

and the vibrational shift operators are given by

$$\hat{G}_n = e^{-\Sigma_i \Phi_{ni}(b_{ni}^{\dagger} - b_{ni})}. \tag{16}$$

The operator $\hat{G}_n^{\dagger}$ creates an excitation along with a cloud of phonons in chromophore n. This represents a vibrationally "dressed" electronic excitation. Using Eq. (8) along with further analysis discussed in Ref. 27, we can write the excitation transfer rate as a correlation function of vibrational shift operators in the Heisenberg representation,

$$W_{nm}(t) = \frac{\lambda_{nm}^2}{\hbar^2}\mathrm{Re}\int_{-\infty}^{\infty} dt e^{i(\tilde{\epsilon}_n - \tilde{\epsilon}_m)/\hbar t}\langle \hat{G}_n^{\dagger}(t)\hat{G}_m(t)\hat{G}_m^{\dagger}\hat{G}_n\rangle_{\mathrm{th}}. \tag{17}$$

The first factor $(\lambda_{nm}^2/\hbar^2)$ in the rate Eq. (17) is an electronic tunneling term that describes the mixing of initial and final states. The operator $\hat{G}_n(t)$ can be written as $e^{iHt/\hbar}\hat{G}_n e^{-iHt/\hbar}$. The correlation function $\langle \hat{G}_n^{\dagger}(t)\hat{G}_m(t)\hat{G}_m^{\dagger}\hat{G}_n\rangle_{\mathrm{th}}$ is thermally averaged over the phonon bath. Vibrational mode i of the nth chromophore segment with frequency ω_{ni} in the correlation function only couples to the vibrational mode i of the mth chromophore segment with the same frequency $\omega_{mi}=\omega_{ni}$. Therefore, the final expression obtained takes the well known form,[27,44]

$$\langle \hat{G}_n^{\dagger}(t)\hat{G}_m(t)\hat{G}_m^{\dagger}\hat{G}_n\rangle_{\mathrm{th}} = \exp\left[-\sum_i \Delta_i(2\bar{n}_i + 1)\right] \times \exp\left[\sum_i (\bar{n}_i\Delta_i e^{i\omega_i t} + (\bar{n}_i + 1)\Delta_i e^{-i\omega_i t})\right], \tag{18}$$

where Δ_i is a dimensionless Huang–Rhys parameter that measures the distance between the minima of displaced parabolas of the vibrational potentials for the nth and mth surfaces,[27,44]

$$\sqrt{\Delta_i} = \left(\frac{g_{ni} - g_{mi}}{\sqrt{8\hbar\omega_i^3}}\right), \tag{19}$$

and $\bar{n}_i$ is the Bose–Einstein thermal occupation of vibrational quanta,[27,44]

$$\bar{n}_i = \frac{1}{\exp(\hbar\omega_i/k_B T) - 1}. \tag{20}$$

C. Energy transfer rates within a dressed eigenstate representation

For the case at hand the electronic couplings occur over a wide range of energies and one cannot comfortably make a

weak coupling approximation. Electronic transitions and, hence, energy transfer events occur within the manifold of electronic eigenstates and one should begin by diagonalizing the electronic parts of Eq. (1),

$$\hat{H}_{el} = T^{\dagger} \cdot H_{el} \cdot T, \tag{21}$$

where T is the unitary transformation matrix that brings H_{el} into diagonal form. We next transform the $H_{el/ph}$ and H_{ph} parts of the Hamiltonian into the electronic eigenbasis,

$$\hat{H}_{el/ph} = T^{\dagger} \cdot H_{el/ph} \cdot T,$$

$$\hat{H}_{ph} = T^{\dagger} \cdot H_{ph} \cdot T, \tag{22}$$

$$A_{\alpha} = (T^{\dagger} \cdot a \cdot T)_{\alpha}.$$

Note, here index α denotes electronic state as opposed to the chromophore site. Finally, we get the transformed Hamiltonian of the system that can be written as a diagonal part,

$$\hat{H} = \sum_{\alpha} E_{\alpha} A_{\alpha}^{\dagger} A_{\alpha} + \sum_{\alpha i} \gamma_{\alpha\alpha i} A_{\alpha}^{\dagger} A_{\alpha} (b_i^{\dagger} + b_i) + \sum_{i} \hbar \omega_i b_i^{\dagger} b_i, \tag{23}$$

and an off-diagonal part $\hat{V}$,

$$\hat{V} = \sum_{\alpha \neq \beta, i} \gamma_{\alpha\beta i} A_{\alpha}^{\dagger} A_{\beta} (b_i^{\dagger} + b_i) + h.c., \tag{24}$$

where $|\alpha\rangle$ represents the electronic eigenstates with vertical energies $\{E_{\alpha}\}$, $\{\gamma_{\alpha\alpha i}\}$ are the diagonal electron-phonon coupling terms, and $\{\gamma_{\alpha\beta i}\}$ are the off-diagonal electron phonon coupling terms. $\{A_{\alpha}^{\dagger}, A_{\beta}\}$ create and destroy excitons with $\{A_{\alpha}, A_{\beta}^{\dagger}\} = \delta_{\alpha\beta}$. We now take the off-diagonal electron-phonon coupling terms as the weak perturbation in order to describe transitions between the electronic eigenstates. Rewriting the Hamiltonian as

$$\bar{H} = \hat{H} + \hat{V}, \tag{25}$$

we can perform a polaron transformation to the electron-phonon Hamiltonian $\bar{H}$. This is achieved with the unitary operator,[37]

$$U = \sum\nolimits_{\alpha} A_{\alpha}^{\dagger} A_{\alpha} e^{-\Sigma_i (\gamma_{\alpha\alpha i}/\omega_i)(b_i^{\dagger} - b_i)}, \tag{26}$$

as

$$\tilde{H} = U^{-1} \cdot \bar{H} \cdot U, \tag{27}$$

where the renormalized electronic energies are[37]

$$\tilde{\epsilon}_{\alpha} = \epsilon_{\alpha} - \sum_{i} \frac{\gamma_{\alpha\alpha i}^2}{\omega}. \tag{28}$$

In Ref. 37 Pereverzev and Bittner used this approach to obtain the following time dependent rate of excitation transfer $W_{\alpha\beta}(t)$ between eigenstates,

$$W_{\alpha\beta}(t) = 2\,\mathrm{Re} \int_0^t d\tau \langle \tilde{M}_{\alpha\beta}(0) \tilde{M}_{\beta\alpha}(\tau) \rangle_{\mathrm{th}} e^{-i(\tilde{\epsilon}_{\beta} - \tilde{\epsilon}_{\alpha})t}, \tag{29}$$

where $\langle \tilde{M}_{\alpha\beta}(0) \tilde{M}_{\beta\alpha}(\tau) \rangle_{\mathrm{th}}$ is the autocorrelation of the shifted electron-phonon operators in the Heisenberg representation. The derivation is given in Ref. 37 and we repeat their main result here,

$$\begin{aligned}\langle \tilde{M}_{\alpha\beta}(0) \tilde{M}_{\beta\alpha}(\tau) \rangle_{\mathrm{th}} = \sum_{i,j} \{ & \gamma_{\alpha\beta i} \gamma_{\beta\alpha j} ((\Delta_{\alpha\beta i}(\bar{n}_i + 1) e^{i\omega_i \tau} e^{-\chi_i \tau} - \Delta_{\alpha\beta i} \bar{n}_i e^{i\omega_i \tau} e^{-\chi_i \tau} + \Omega_{\alpha\beta i}) \\ & \times (\Delta_{\alpha\beta j}(\bar{n}_j + 1) e^{i\omega_i \tau} e^{-\chi_i \tau} - \Delta_{\alpha\beta j} \bar{n}_j e^{i\omega_i \tau} e^{-\chi_i \tau} \Omega_{\alpha\beta j}) + \delta_{ij}(\bar{n}_i + 1) e^{i\omega_i \tau} e^{-\chi_i \tau} + \delta_{ij} \bar{n}_i e^{i\omega_i \tau} e^{-\chi_i \tau}) q_{\alpha\beta}(\tau) f_{\alpha\beta}(\tau) \},\end{aligned} \tag{30}$$

where

$$\Delta_{\alpha\beta i} = \frac{(\gamma_{\alpha\alpha i} - \gamma_{\beta\beta i})}{\omega_i}, \tag{31}$$

$$\Omega_{\alpha\beta i} = \frac{(\gamma_{\alpha\alpha i} + \gamma_{\beta\beta i})}{\omega_i}, \tag{32}$$

$$\bar{n}_i = \frac{1}{\exp(\hbar \omega_i / k_B T) - 1}, \tag{33}$$

$$q_{\alpha\beta}(\tau) = e^{i\Sigma_j \Delta_{\alpha\beta j} e^{-\chi_j \tau} \sin(\omega_j \tau)}, \tag{34}$$

and

$$f_{\alpha\beta}(\tau) = e^{-2\Sigma_j (n_j + 1/2) \Delta_{\alpha\beta j}^2 (1 - e^{-\chi_j \tau} \cos(\omega_j \tau))}. \tag{35}$$

The golden-rule rate is then given by

$$\lim_{t \to \infty} W_{\alpha\beta}(t) = \bar{W}_{\alpha\beta}, \tag{36}$$

assuming that the correlation function in Eq. (29) converges to 0 at long enough time. However, since we have only a few phonon modes per chromophore segment, there is the possibility that recurrences can prevent the long-time decay of $\langle \tilde{M}_{\alpha\beta}(0) \tilde{M}_{\alpha\beta}(\tau) \rangle$. As such, we have assumed a phonon lifetime χ_j^{-1} of 551 fs associated with three chromophore phonon modes, which corresponds to a phonon lifetime width of ~60 wave number (cm^{-1}). In order to ensure our results are not sensitive to our choice of phonon lifetime, we compare results for different values of χ_j over a range of lifetimes from 50% χ to 200% χ. Figure 5 shows a plot of the autocorrelation function $C(t) = \langle \tilde{M}_{\alpha\beta}(0) \tilde{M}_{\beta\alpha}(\tau) \rangle_{\mathrm{th}}$ between two coupled electronic states of our system at $T = 300$ K. The decay of the electron-phonon autocorrelation function gives

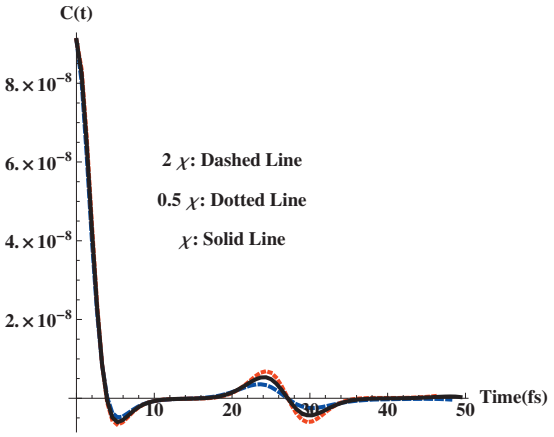

FIG. 5. Plot of electron-phonon autocorrelation function in the dressed eigenstate representation [Eq. (30)]: $C(t)=\langle \tilde{M}_{\alpha\beta}(0)\tilde{M}_{\beta\alpha}(\tau)\rangle$ with respect to phonon lifetime χ for states #1 and #2 of polymer chain C at 300 K.

the electronic decoherence time.[45–47] For the case shown in Fig. 5, the initial decay occurs well within 5 fs with a small recurrence between 20 and 30 fs. This suggests that the bath correlation times are significantly shorter than the transfer times between the states.[48] Therefore, we can safely model the exciton transfer dynamics as an incoherent process.

III. RESULTS AND DISCUSSION

Anisotropy decay is induced by exciton migration along the chain. For a disordered system, the initial anisotropy[19,49,50] is equal to ~0.4. In the results shown here, we normalize the anisotropy to an initial value of 1.[20] The anisotropy decay for each chain is realized by averaging over 100 replication sets. Figure 6 displays the simulated anisotropy decay upon averaging in the first 400 ps after the primary photoexcitation for three representative PPV conjugated polymer chains as computed using the two different approximations for the hopping rates. The calculated anisotropy for chain A in the dressed eigenstate representation [Fig. 6(a)] reaches half of its initial value after less than

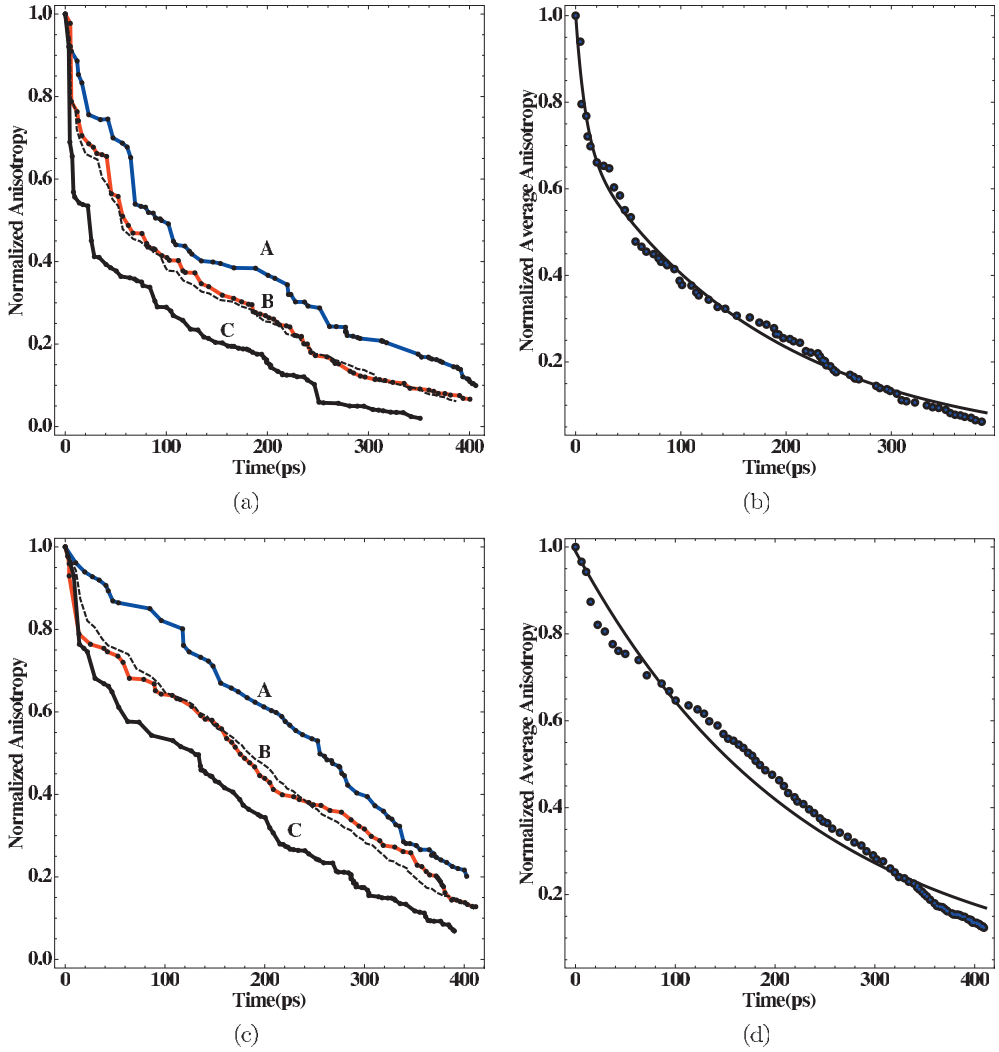

FIG. 6. Normalized anisotropy decay upon averaging for three representative PPV polymer chains A, B, and C at 300 K. The dressed eigenstate representation: (a) the black dashed line is the anisotropy decay averaged over three chains and (b) the biexponential fit to the average anisotropy decay (RSquared =0.9973). It shows two time constant, a faster component (τ_1=9.54 ps), and a slower component (τ_2=183 ps). The chromophore site (localized) representation: (c) the black dashed line is averaged over three chains and (d) an exponential fit to the average anisotropy decay (RSquared=0.9925). Average decay line shows a single time constant (τ=217 ps).

100 ps, whereas in the localized picture [Fig. 6(c)], a much slower decay 255 ps is observed. The calculated anisotropy for chain *B* in the dressed eigenstate representation [Fig. 6(a)] shows a decay which reaches half of its initial value after less than ~60 ps, whereas in the localized representation [Fig. 6(c)], a slower decay ~180 ps is observed. Chain *C* shows a much faster anisotropy decay in the dressed eigenstate representation, which reaches half of its value after less than 25 ps compared to 130 ps in the localized representation. Thus we conclude that accounting properly for delocalization over multiple chromophore units generally leads to more efficient energy transfer through the system.

It has been reported in Refs. 16 and 49 that conformational disorder is the important factor in the long time anisotropy decay and there is a dependence on the radius of gyration of the chain. As shown in Fig. 6, chains with the larger radii of gyration (*A* and *B*) show slower average anisotropy decay than chain *C* in both representations. The most extended chain gives the slowest calculated anisotropy decay on average because the extended polymer chain contains a broad distribution of chromophore lengths, electronic coupling parameters λ_{nm}, and energy mismatches among the chromophores.[16] The chain with the smallest radius contains a higher percentage of shorter chromophores that are more likely to lie adjacent to one other on the chain.[16] This leads to a larger number of more strongly coupled chromophores, which favors excitation relaxation to the lower states, and an efficient energy transfer in the system.

Figures 6(a) and 6(c) also show the average depolarization for the dressed eigenstate and chromophore site representation as obtained by averaging over conformations of the three representative polymer chains. The average decay for the dressed eigenstate case [Fig. 6(b)] displays depolarization with two time constants: a faster component (τ_1=9.54 ps) due to short-range strong electronic interactions and a slower component (τ_2=183 ps) due to long-range weak electronic interactions.[51] The shorter time scale component can be attributed to rapid hopping between states that are localized within a small neighborhood around the original excitation. This leads to a rapid depolarization of the initial excitation. On the other hand, the average anisotropy decay in the chromophore site representation [Fig. 6(d)] shows a single decay constant (τ=217 ps) for a similar loss of anisotropy.

Ruseckas and co-workers[50,52] reported that the long-time decay is characteristic of intrachain exciton interaction and can be attributed to the incoherent excitation transfer *along* the disordered polymer chain. In contrast, our results indicate that the long-time decay component can be attributed to less-frequent longer-range (through-space) hopping from the original excitation region to more remote regions of the polymer chain. This is illustrated in Fig. 7 where we have highlighted the initial exciton (in this case state #60 of chain C) as well as four other states (#35, #37, #38, and #1) in the dressed eigenstate representation. The initial exciton eventually migrates to lower energy states over the course of a single run. This migration is largely *through-space* rather than through-bonds connecting neighboring segments.

Figure 8(a) shows a plot of the exciton energy versus time in the dressed eigenstate representation for an exciton

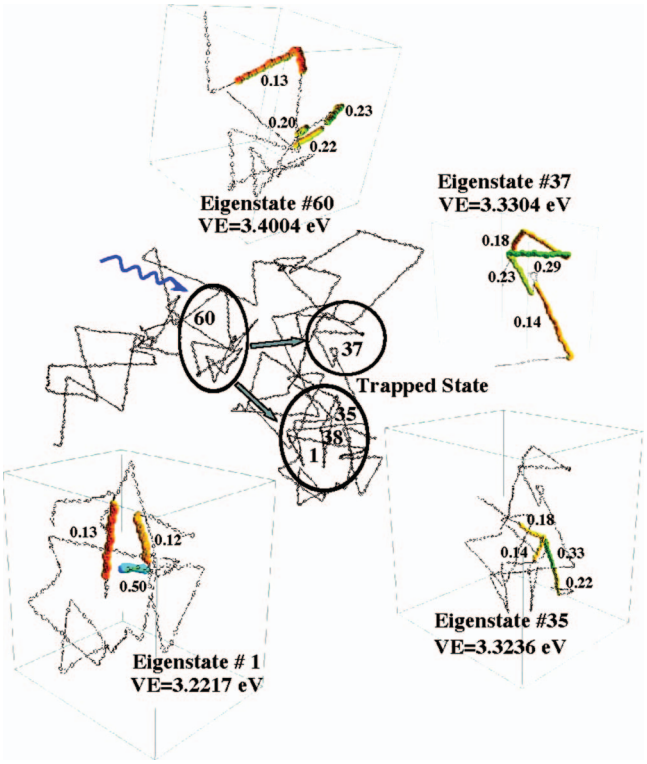

FIG. 7. Graphical picture for the migration of an initial photoexcitation from state #60 to the kinetically trapped states. VE denotes the vertical excitation energy in eV. The coloring along the chain is based on the amplitude of eigenstate coefficients projected on to the chromophore basis sets.

initiated in state #60 of chain C. The plot gives insight into a range of states visited by the exciton as it migrates. The majority of the trajectories initiated from state #60 become trapped into the range of states from #32 to #38 after 500 ps. However, a few trajectories do escape to the lower energy states (#12 or #13). In comparison, in Fig. 8(b), we initiated the exciton in state #126 of chain C. Again, within 500 ps, the exciton localizes into the range of states from #85 to #98.

From a thermodynamic point of view, the initial excitation should eventually find the lowest energy state (#1). Referring back to the density of states (Fig. 4), one can see that the density of states for the lowest energy states is quite high. However, these states also have the largest IPR, meaning that almost all of them are composed of a single-chromophore segment. These segments, in turn, correspond to the longer contiguous π-conjugated domains along the chain itself. These long, low energy segments are generally isolated from each other and consequently, their coupling to other lower energy states is extremely weak. Once the exciton locates one of these states, it becomes unlikely that it will be able to make a long-distance hop to another low energy state within its radiative lifetime. Hence, the exciton can become kinetically trapped. It has been shown to exist previously that the trapping of excitation occurs when the hopping rate to lower-energy sites is longer than the radiative lifetime of the exciton, and to explain quantitatively the anomalous temperature dependence of the Stokes shift measured in molecular J-aggregates of the THIATS (3,3′-bis(sulfopropyl)-5,5′-dichloro-9-ethylthiacarbocyanine).[53,54]

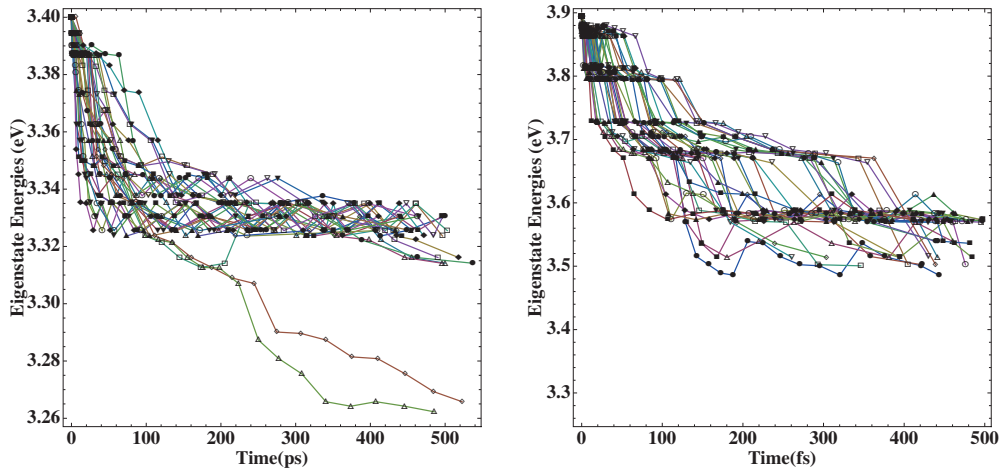

(a)Initial Eigenstate Index = #60 (b)Initial Eigenstate Index = #126

FIG. 8. Exciton energy vs time over the course of multiple hopping trajectories for chain C starting from two different initial states in the dressed eigenstate representation (a) state #60 and (b) state #126.

IV. CONCLUSIONS

In this paper, we have compared two models of energy transfer within a conjugated polymer network starting from a common Hamiltonian and computed transfer rates within first-order perturbation theory. In the first case, we took the more traditional route and treated the bare electronic coupling as the perturbation as in a molecular crystal model. However, within a polymer network, one cannot safely assume the weak-coupling limit between all pairs of chromophores. As an improvement over the molecular crystal model, we first diagonalized the electronic part of the Hamiltonian and then treated the much-weaker nonadiabatic electron-phonon coupling as the perturbation.

In the previous work by Dykstra *et al.*,[16] we modeled the short time dynamics of the exciton by assuming that the *initial* excitation was localized on a single chromophore segment and that rapid fluorescence depolarization was the result of the delocalization and relaxation of the chromophore into an eigenstate. Our current model allows us to consider the longer time migration at that state through the polymer itself. Following localization in an eigenstate, the exciton can make a series of rapid hops within the neighborhood of the initial excitation. This results in a rapid depolarization on the time scale of ≈ 10 ps. Following this initial series of hops, the exciton can make a series of longer ranged hops to lower energy states on the time scale of ≈ 200 ps. However, even though the density of states is highest for the lowest energy states, such states are generally composed of a single contiguous π conjugated segment and are essentially decoupled from each other. Consequently, the exciton can become kinetically trapped in such states since the time scale for hopping to the lowest energy state can be comparable to its radiative lifetime (≈ 500 ps to 1 ns).

In the functional form of PPV and poly[2-methoxy-5-((2-ethylhexyl)oxy)-1,4-phenylenevinylene] (MEH-PPV) materials, the situation is very different due to a local disorder and redshift effect. These redshift effects are an intrinsic properties of the PPV and MEH-PPV polymers.[55] Therefore, the flexible disorder and a redshift emission in these kind of materials have a dramatic effect on the energy transfer, as it has been reported in Ref. 15 that the conformations of MEH-PPV chains show an increased energy transfer efficiency in the films as compared to the solutions due to redshifted fluorescence and a large Stokes' shifts. Certainly, our results are highly sensitive to the secondary structure of the polymer chain and we have chosen a relatively small sample of possible polymer structures. Furthermore, we have only considered energy transfer as occurring within a single contiguous polymer chain. In a thin film, multiple chains would be intermingled and intertwined. However, since we have assumed that the polymer chains themselves remain more or less static over a 1 ns time scale, we can consider even a polymer thin film as consisting of a disordered array of coupled chromophore segments. Thus, even within the limitations of our basic model, our results here and in Ref. 16 underscore the fact that the quantum dynamics of energy diffusion occurs on a wide range of time scales, each corresponding to specific steps of the energy transfer and relaxation processes within a conjugated polymer.

ACKNOWLEDGMENTS

This work was supported in part by the National Science Foundation (Grant No. CHE-0712981) and the Robert A. Welch Foundation (Grant No. E-1337). G.D.S. acknowledges the support of an EWR Steacie Memorial Fellowship. The work in Mons is partly supported by the Belgian Federal Government "Interuniversity Attraction Pole in Supramolecular Chemistry and Catalysis, PAI 5/3;" the European-funded projects MINOTOR (Grant No. FP7-NMP-228424), MODECOM (Grant No. NMP3-CT-016434), and ONE-P (Grant No. NMP3-LA-2008-212311); and the Belgian National Fund for Scientific Research (FNRS/FRFC). D.B. is a FNRS Research Fellow.

[1] J. H. Burroughes, D. D. C. Bradley, A. R. Brown, R. N. Marks, K. Mackay, R. H. Friend, P. L. Burns, and A. B. Holmes, Nature **347**, 539 (1990).

[2] I. D. W. Samuel, G. Rumbles, and R. H. Friend, *Primary Photoexcitations in Conjugated Polymers: Molecular Model versus Band Model, 9* (World Scientific, Singapore, 1997).
[3] A. C. Arias, J. D. MacKenzie, R. Stevenson, J. J. M. Halls, M. Inbasekaran, E. P. Woo, D. Richards, and R. H. Friend, Macromolecules **34**, 6005 (2001).
[4] G. Malliaras and R. H. Friend, Phys. Today **58**, 53 (2005).
[5] S. A. Jenekhe and J. A. Osaheni, Science **265**, 765 (1994).
[6] G. Hadziioannou and G. Malliaras, *Semiconducting Polymers: Chemistry, Physics and Engineering*, 2nd ed., Vols. I–II (Wiley-VCH, Weinheim, 2007).
[7] J.-L. Bredas, D. Beljonne, V. Coropceanu, and J. Cornil, Chem. Rev. **104**, 4971 (2004).
[8] B. J. Schwartz, Annu. Rev. Phys. Chem. **54**, 141 (2003).
[9] G. D. Scholes and G. Rumbles, Nature Mater. **5**, 683 (2006).
[10] M.-H. Chang, M. Hoffmann, H. L. Anderson, and L. M. Herz, J. Am. Chem. Soc. **130**, 10171 (2008).
[11] C. L. Gettinger, A. J. Heeger, J. M. Drake, and D. J. Pine, J. Chem. Phys. **101**, 1673 (1994).
[12] B. Van Averbeke and D. Beljonne, J. Phys. Chem. A **113**, 2677 (2009).
[13] G. C. Claudio and E. R. Bittner, J. Chem. Phys. **115**, 9585 (2001).
[14] G. C. Claudio, Ph.D. thesis, University of Houston, 2003.
[15] T. E. Dykstra, V. Kovalevskij, X. Yang, and G. D. Scholes, Chem. Phys. **318**, 21 (2005).
[16] T. E. Dykstra, E. Hennebicq, D. Beljonne, J. Gierschner, G. Claudio, E. R. Bittner, J. Knoester, and G. D. Scholes, J. Phys. Chem. B **113**, 656 (2009).
[17] K. Brunner, A. Tortschanoff, C. Warmuth, H. Bassler, and H. F. Kauffmann, J. Phys. Chem. B **104**, 3781 (2000).
[18] G. D. Scholes, Annu. Rev. Phys. Chem. **54**, 57 (2003).
[19] M. H. Chang, M. J. Frampton, H. L. Anderson, and L. M. Herz, Phys. Rev. Lett. **98**, 027402 (2007).
[20] K. M. Gaab and C. J. Bardeen, J. Phys. Chem. A **108**, 10801 (2004).
[21] M. M. L. Grage, T. Pullerits, A. Ruseckas, M. Theander, O. Inganäs, and V. Sundström, Chem. Phys. Lett. **339**, 96 (2001).
[22] E. Collini and G. D. Scholes, Science **323**, 369 (2009).
[23] J.-L. Bredas and R. Silbey, Science **323**, 348 (2009).
[24] S. Karabunarliev and E. R. Bittner, J. Chem. Phys. **118**, 4291 (2003).
[25] S. Karabunarliev and E. R. Bittner, J. Phys. Chem. B **108**, 10219 (2004).
[26] R. Silbey, Annu. Rev. Phys. Chem. **27**, 203 (1976).
[27] G. C. Schatz and M. A. Ratner, *Quantum Mechanics in Chemistry* (Dover, New York, 2002).
[28] T. F. Soules and C. B. Duke, Phys. Rev. B **3**, 262 (1971).
[29] S. Fischer and S. A. Rice, J. Chem. Phys. **52**, 2089 (1970).
[30] M. K. Grover and R. Silbey, J. Chem. Phys. **52**, 2099 (1970).
[31] F. C. Spano, J. Chem. Phys. **122**, 234701 (2005).
[32] G. C. Claudio and E. R. Bittner, J. Phys. Chem. A **107**, 7092 (2003).
[33] S. Karabunarliev and E. R. Bittner, Phys. Rev. Lett. **90**, 057402 (2003).
[34] S. Karabunarliev, E. R. Bittner, and M. Baumgarten, J. Chem. Phys. **114**, 5863 (2001).
[35] A. Blumen, J. P. Lemaistre, and I. Mathlouthi, J. Chem. Phys. **81**, 4610 (1984).
[36] H. Fidder, J. Knoester, and D. A. Wiersma, J. Chem. Phys. **95**, 7880 (1991).
[37] A. Pereverzev and E. R. Bittner, J. Chem. Phys. **125**, 104906 (2006).
[38] S. D. Druger, M. A. Ratner, and A. Nitzan, Phys. Rev. B **31**, 3939 (1985).
[39] A. K. Harrison and R. Zwanzig, Phys. Rev. A **32**, 1072 (1985).
[40] D. P. Landau and K. Binder, *A Guide to Monte Carlo Simulations in Statistical Physics* (Cambridge University Press, Cambridge, 2005).
[41] H. Bassler, Phys. Status Solidi B **175**, 15 (1993).
[42] D. Yarkony and R. Silbey, J. Chem. Phys. **65**, 1042 (1976).
[43] D. R. Yarkony and R. Silbey, J. Chem. Phys. **67**, 5818 (1977).
[44] S. Karabunarliev and E. R. Bittner, J. Chem. Phys. **119**, 3988 (2003).
[45] E. R. Bittner and P. J. Rossky, J. Chem. Phys. **107**, 8611 (1997).
[46] V. May and O. Kuhn, *Charge and Energy Transfer Dynamics in Molecular Systems* (Wiley, New York, 2004).
[47] A. Nitzan, *Chemical Dynamic in Condensed Phases*, 1st ed. (Oxford University Press, New York, 2006).
[48] C. R. Gochanour, H. C. Andersen, and M. D. Fayer, J. Chem. Phys. **70**, 4254 (1979).
[49] M. M.-L. Grage, P. W. Wood, A. Ruseckas, T. Pullerits, W. Mitchell, P. L. Burn, I. D. W. Samuel, and V. Sundstrom, J. Chem. Phys. **118**, 7644 (2003).
[50] A. Ruseckas, P. Wood, I. D. W. Samuel, G. R. Webster, W. J. Mitchell, P. L. Burn, and V. Sundström, Phys. Rev. B **72**, 115214 (2005).
[51] S. Lakshmi, A. Datta, and S. K. Pati, Phys. Rev. B **72**, 045131 (2005).
[52] G. Lanzani, G. Cerullo, C. Brabec, and N. S. Sariciftci, Phys. Rev. Lett. **90**, 047402 (2003).
[53] M. Bednarz, V. A. Malyshev, and J. Knoester, Phys. Rev. Lett. **91**, 217401 (2003).
[54] M. Bednarz, V. A. Malyshev, and J. Knoester, J. Chem. Phys. **120**, 3827 (2004).
[55] A. C. Grimsdale, K. Leok Chan, R. E. Martin, P. G. Jokisz, and A. B. Holmes, Chem. Rev. **109**, 897 (2009).